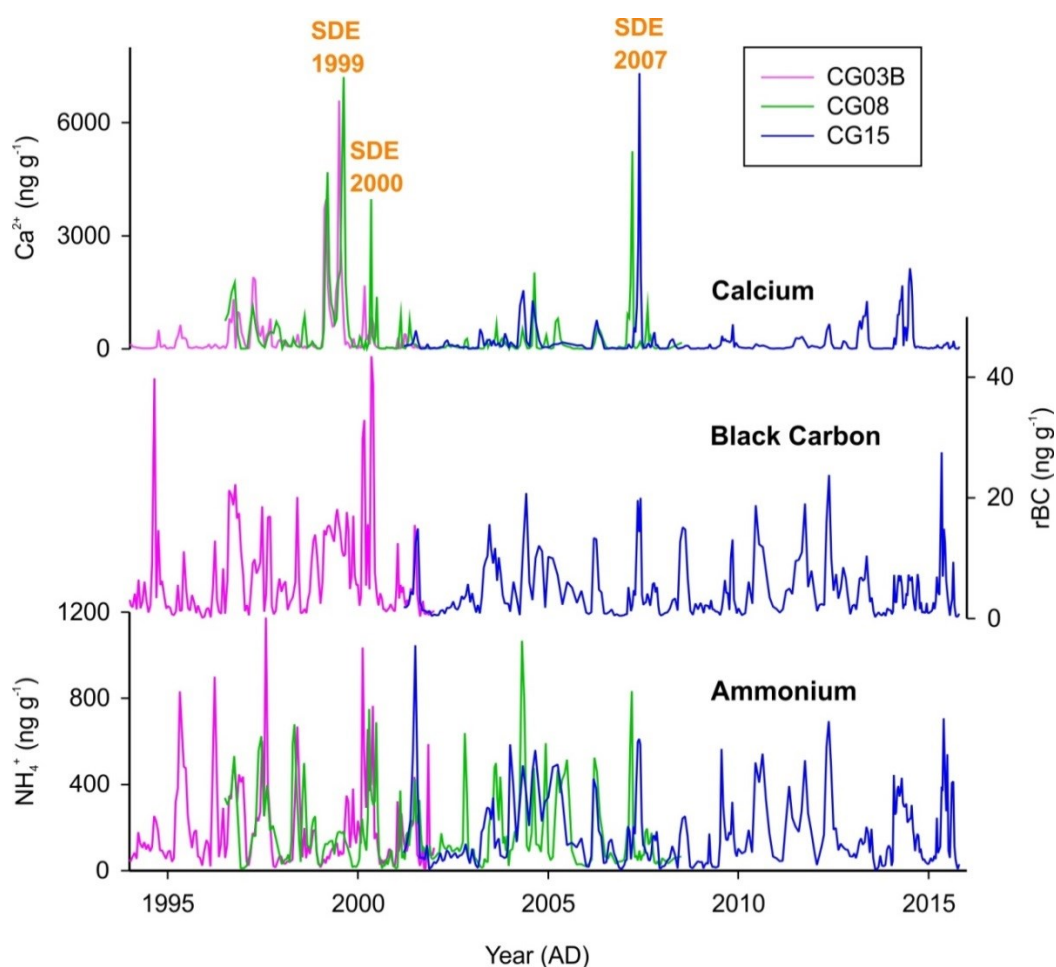


5 **Supplementary Fig. S1:** Colle Gnifetti timescale **a)** Depth-age relationship for CG03 based on combining annual-layer counting with distinctive reference horizons (Jenk et al., 2009); **b)** CG15 NH_4^+ concentrations used for extending the chronology into the present. **c)** Volcano Index (defined as $\text{Volcano Index} = [\text{SO}_4^{2-}]^2/[\text{Ca}^{2+}]$) and Ca^{2+} concentrations used to identify volcanic eruptions and historic Saharan dust events (Wagenbach et al., 1996; Oeschger et al., 1977).

Supplementary Table S1: Age markers for the Colle Gnifetti ice cores.

Type of Age Marker	Parameter	Year (AD)	CG03A Depth (m)	CG03B Depth (m)
SDE 1977	Ca ²⁺ , Fe	1977	18.90	18.88
NWT	³ H	1963	24.45	n.a.
SDE 1947	Ca ²⁺ , Fe	1947	29.23	29.32
SDE 1936	Ca ²⁺ , Fe	1936	31.96	32.03
Katmai 1912	SO ₄ ²⁻ , SO ₄ ²⁻ /Ca ²⁺	1912	37.31	37.44
SDE 1901	Ca ²⁺ , Fe	1901	39.20	39.28
SDE 1863	Ca ²⁺ , Fe	1863	44.36	44.46
Tambora 1815	SO ₄ ²⁻ , SO ₄ ²⁻ /Ca ²⁺	1816	49.79	49.79
Laki 1783	SO ₄ ²⁻ , SO ₄ ²⁻ /Ca ²⁺	1783	53.50	53.42
Bedrock		-17000	80.18	81.14

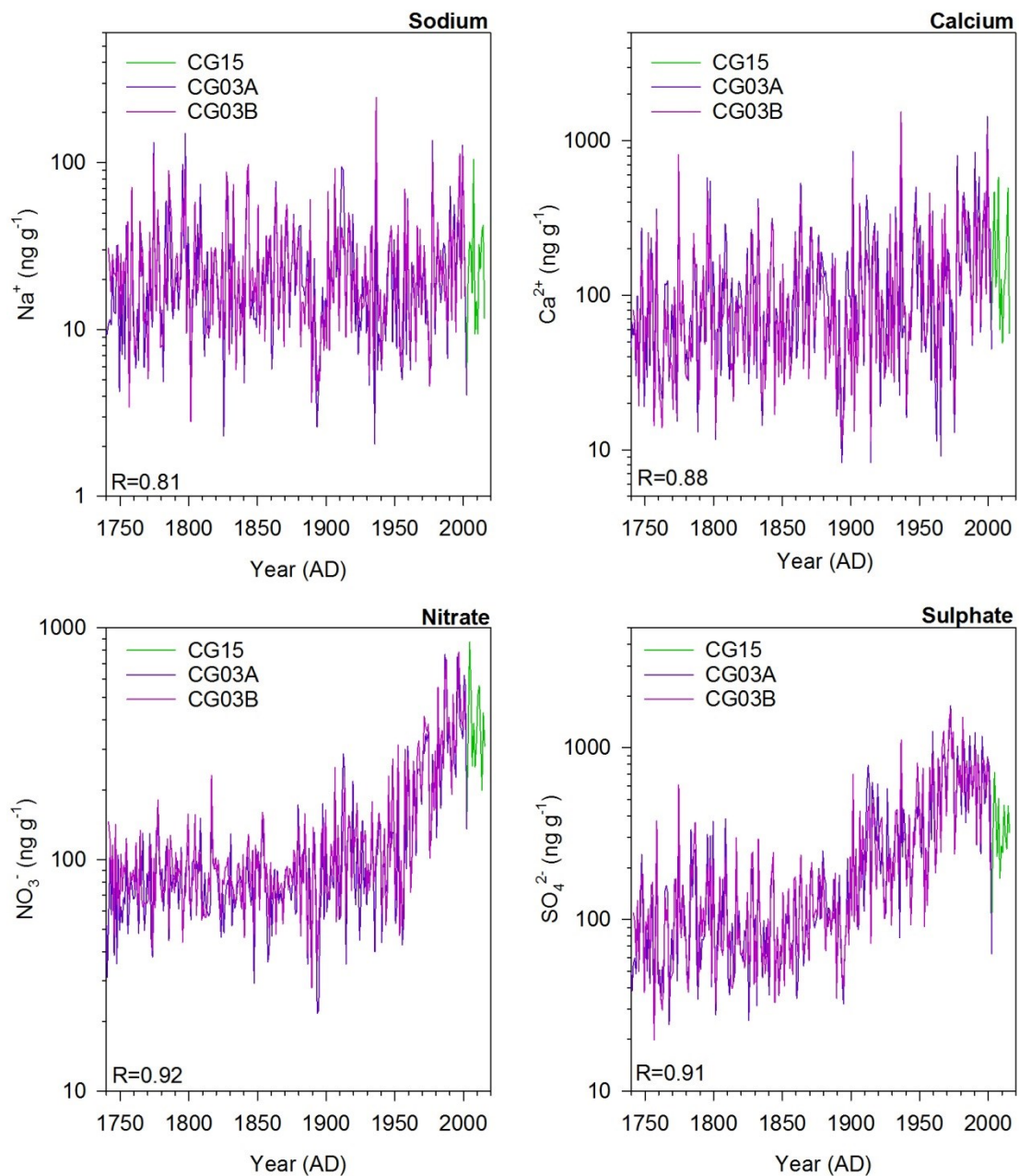
SDE = Historic Saharan Dust Event (Wagenbach et al., 1996; Oeschger et al., 1977); NWT = Maximum of northern hemisphere nuclear weapon testing; n.a. = not analyzed



5

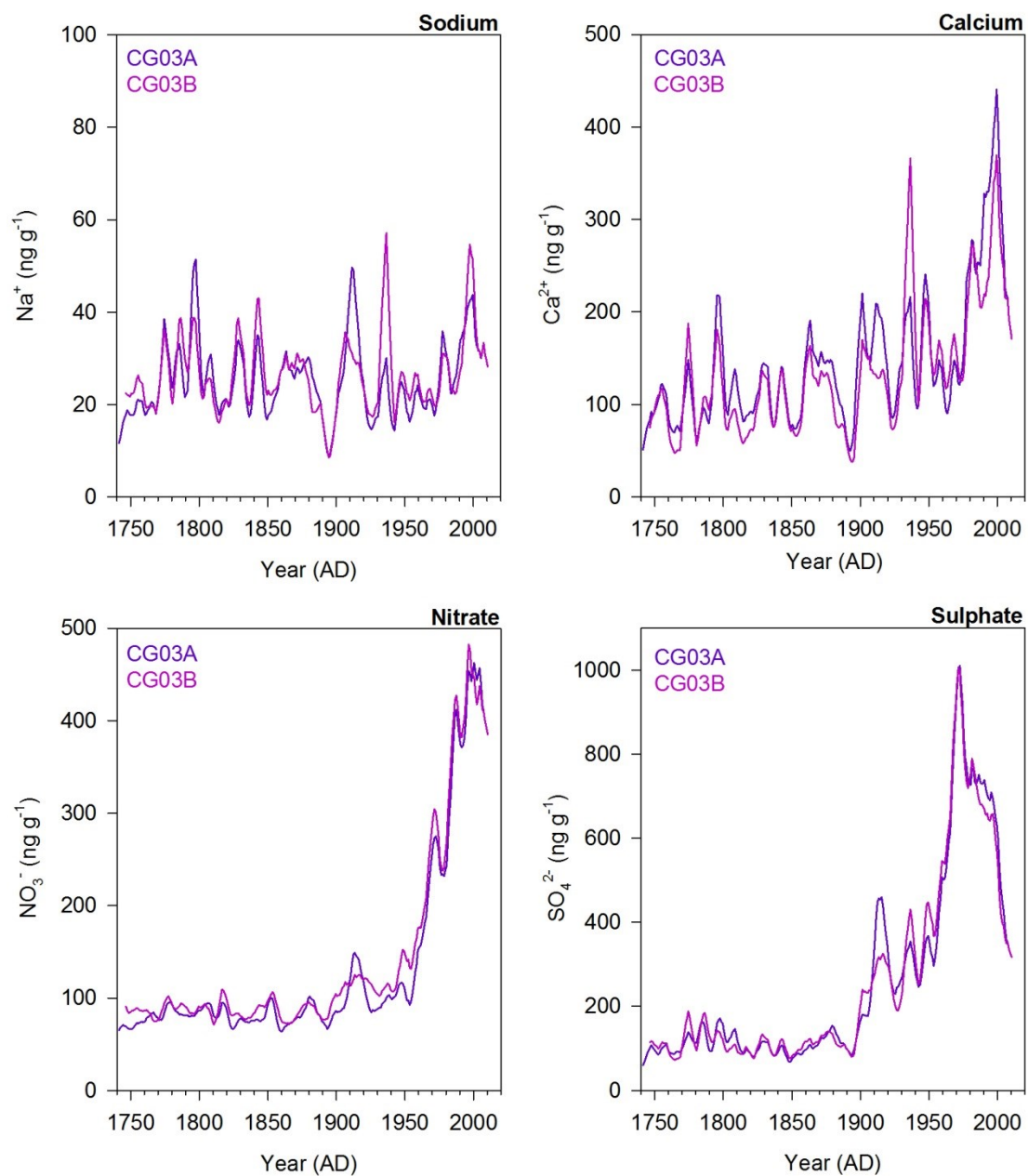
Supplementary Fig. S2: Comparison of selected tracers for the three ice/firn cores CG03B, CG08 and CG15. CG03B was dated by synchronization with CG03A, whereas CG08 and CG15 were dated by counting annual layers.

10



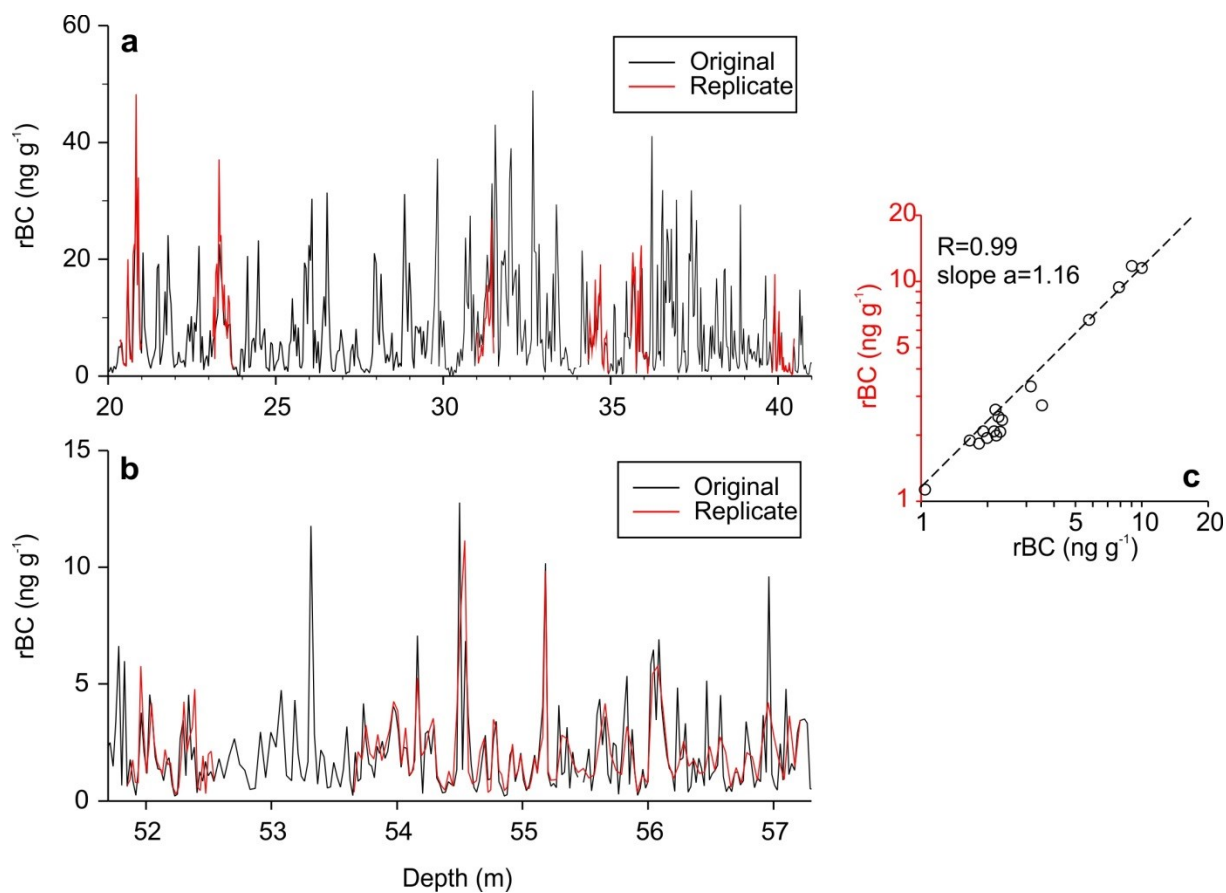
Supplementary Fig. S3: Annual concentrations of selected tracers for the new ice core CG15 and the two parallel cores CG03A and CG03B (1741-2015 AD) with Pearson's correlation coefficient (R) indicated.

5

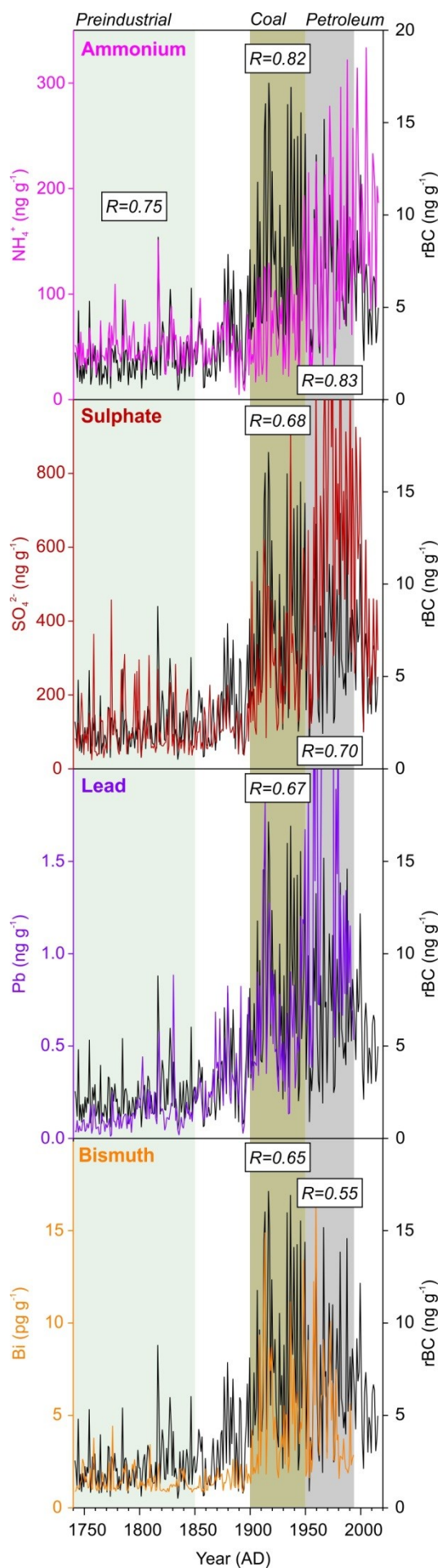


Supplementary Fig. S4: Concentrations of selected tracers for the two parallel cores CG03A and CG03B (1741-2002 AD) extended using CG15 (2003-2014 AD). All records were smoothed with an 11-year filter.

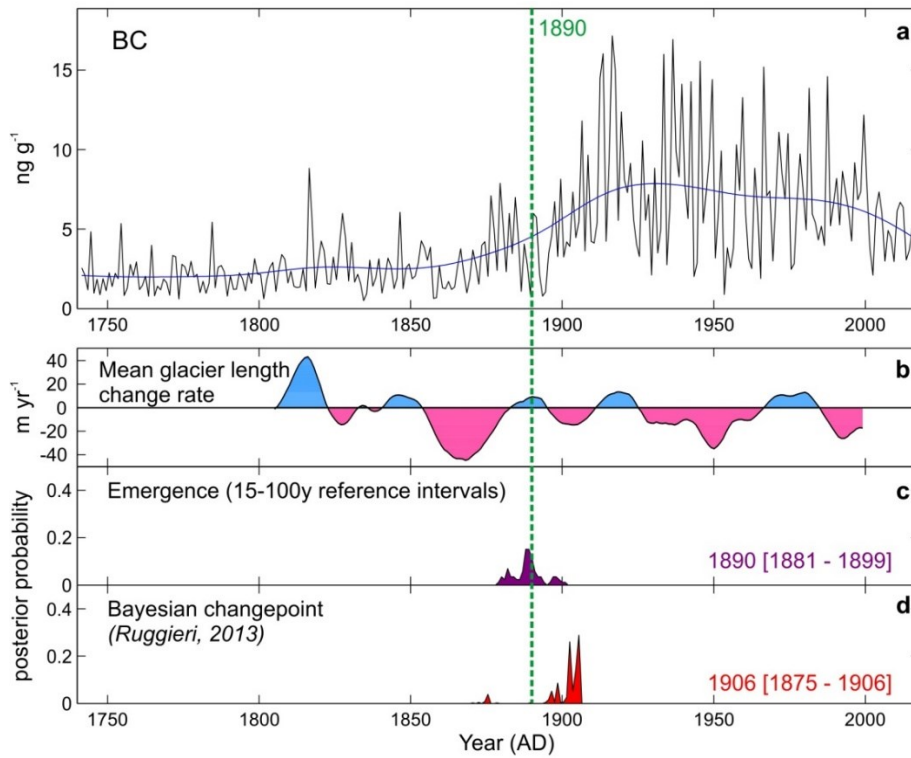
5



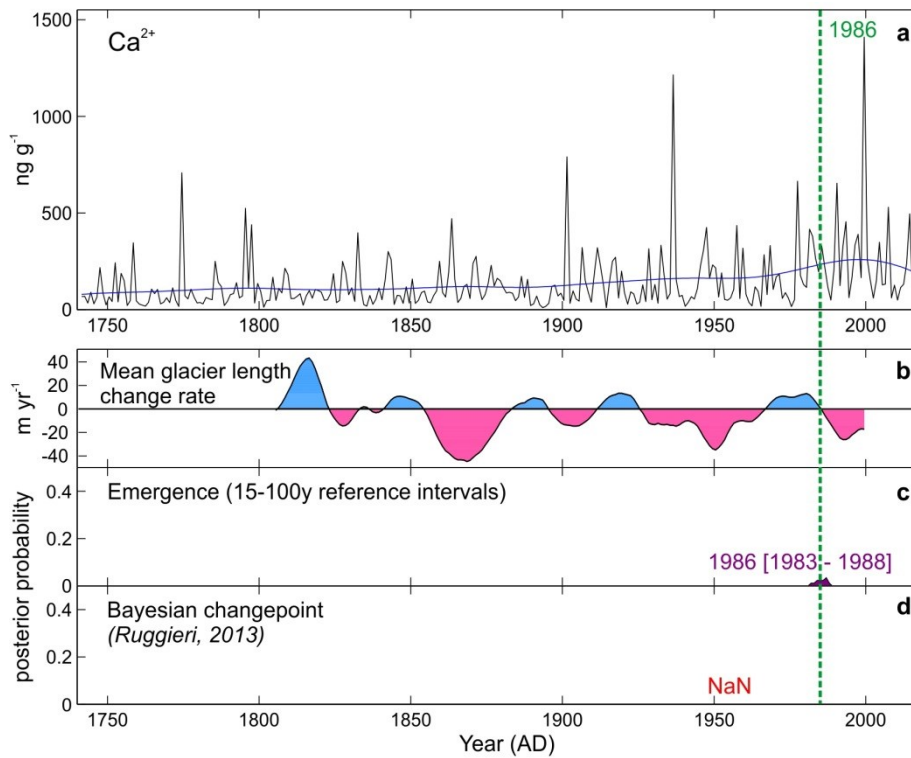
Supplementary Fig. S5: a) Comparison of original analyses and replicate analyses for CG03 **a)** during the industrial period (1888-1975 AD) and **b)** during the preindustrial period (1740-1799 AD).
 5 **c)** mean concentrations determined for all ice-core sections with available replication samples with a linear fit against mean values from the original analysis.



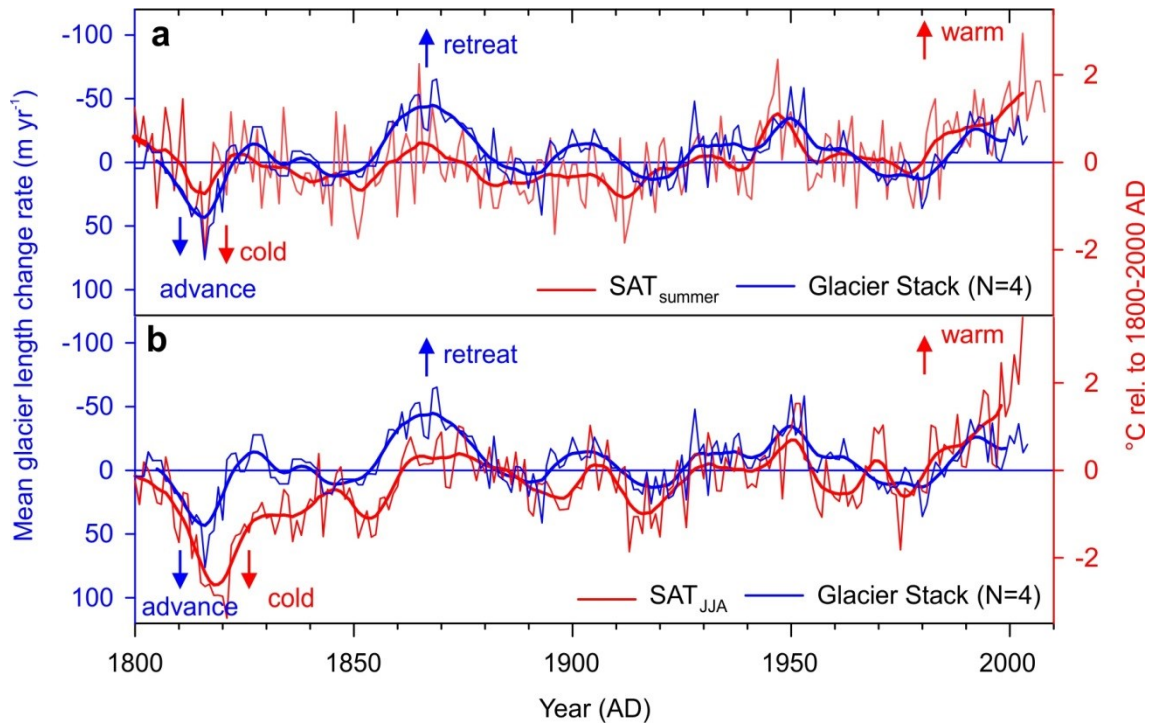
Supplementary Fig. S6: Colle Gnifetti rBC record compared with selected glaciochemical and trace element records. *Pearson's* correlation coefficients ($P < 0.0001$; 1-sided) are displayed for time periods dominated by preindustrial emissions (1741-1850 AD), coal burning (1901-1950 AD) and burning of petroleum products emissions (1951-1993 AD), respectively.



Supplementary Fig. S7: As Fig. 7 but for total BC concentrations



5 Supplementary Fig. S8: As Fig. 7 but for total Ca^{2+} concentrations



5 **Supplementary Fig. S9: a)** Smoothed and annual resolution mean glacier length change rates of the *Glacier Stack* and equally resolved surface air temperature anomalies for the summer half year (SAT_{summer}) from the Greater Alpine Region HISTALP station network (Böhm et al., 2010); note that the curves are displayed inverse compared to Fig. 8; **b)** the same *Glacier Stack* curves compared with a June-August surface air temperature reconstruction for the greater Alpine region based on tree-rings (Büntgen et al., 2011).

10 **Supplementary References:**

Büntgen, U., Tegel, W., Nicolussi, K., McCormick, M., Frank, D., Trouet, V., Kaplan, J. O., Herzig, F., Heussner, K. U., Wanner, H., Luterbacher, J., and Esper, J.: 2500 Years of European Climate Variability and Human Susceptibility, *Science*, 331, 578-582, 2011.